

# In situ investigations on a Li-rich Mn-Ni layered oxide for Li-ion battery

Loïc Simonin<sup>\*a</sup>, Jean-François Colin<sup>a</sup>, Vincent Ranieri<sup>b</sup>, Emmanuel Canévet<sup>a</sup>, Jean-Frédéric Martin<sup>a</sup>, Carole Bourbon<sup>a</sup>, Carsten Baetz<sup>c</sup>, Pierre Strobel<sup>d</sup>, Lise Daniel<sup>a</sup> and Sébastien Patoux<sup>a</sup>

<sup>a</sup> CEA-LITEN, 17 rue des Martyrs, 38054 Grenoble CEDEX 9, France.. Fax: +33 4 3878 4383 Tel: +33 4 38 78 04 27 E-mail: loic.simonin@cea.fr

<sup>b</sup> CEA-INAC, 17 rue des Martyrs, 38054 Grenoble CEDEX 9, France.

<sup>c</sup> Institute of Ion Beam Physics and Materials Research, Helmholtz-Zentrum Dresden Rossendorf, Dresden, D-01314, Germany

<sup>d</sup> CNRS-Institut Neel, 25 avenue des Martyrs 38042 Grenoble CEDEX 9, France.

## Introduction

In order to satisfy new energy storage requirements resulting from the growing need for electrical transportation, many efforts are put into the development of Li-ion batteries<sup>1-3</sup>. For automotive application, higher autonomy is required. To face this challenge, it is important to develop high capacity cathode materials that are cheap, safe, and with a good cycling stability. In that purpose, Mn-based Li-rich layered oxides with the general formula  $\text{Li}[\text{Li}_x\text{M}_{1-x}]\text{O}_2$  ( $\text{M} \Leftrightarrow$  transition metal elements,  $0 < x < 1/3$ ) are very promising candidates; indeed, it was reported that they can reach capacities higher than  $250 \text{mAh.g}^{-1}$  when it is cycled beyond 4.5V vs.  $\text{Li}^+/\text{Li}^{4-6}$ . However, they suffer a high irreversible capacity during the first cycle. The reasons for both the high initial capacity and the high irreversibility are still unclear, although the mechanism of lithium insertion-extraction during the first cycle has been studied by several groups<sup>7-14</sup>. Considering that all transition metals can only oxidise to the 4+ oxidation state, the amount of exchanged lithium should not exceed 0.4 per unit formula, which corresponds to a specific capacity of only  $126 \text{mAh.g}^{-1}$ . The general explanation considers a lithium extraction beyond total oxidation of transition metals, accompanied by oxygen extraction ( $\text{O}^{2-} \rightarrow \frac{1}{2}\text{O}_2 + 2\text{e}^-$ ) at high potential<sup>7,9,12</sup>. As the shape of the cycling curves changes after the first charge, it is believed that this high potential oxygen evolution is a driving force for a structural rearrangement. In order to get a better insight on these structural changes, several *in situ* experiments have been performed on  $\text{Li}[\text{Li}_{0.2}\text{Mn}_{0.61}\text{Ni}_{0.18}\text{Mg}_{0.01}]\text{O}_2$  in this study at BM20 for X-Ray diffraction and BM30B for X-ray Absorption.

## Materials and Methods

The compound with the formula  $\text{Li}[\text{Li}_{0.2}\text{Mn}_{0.61}\text{Ni}_{0.18}\text{Mg}_{0.01}]\text{O}_2$  was synthesised by an all solid state route. Mn, Ni, Mg, and Li carbonates were intimately mixed in n-hexane in a stoichiometric ratio in a Retsch centrifuge ball Mill. The obtained mixture was then heated at  $1000^\circ\text{C}$  for 24h in air and then cooled rapidly to room temperature.

## *In situ* X-ray Diffraction (XRD)

For the cell dedicated to XRD measurements, the final surface density of the electrode was around  $25 \text{mg.cm}^{-2}$  (86wt% active material). Rectangular electrodes of  $2 \text{cm}^2$  were cut out and dried under vacuum at  $60^\circ\text{C}$  for 48h. The assembly of the Li-rich Layered oxide/ Li metal pouch cells was performed in an Argon filled glove box. A polypropylene membrane (Celgard® 2400) was used as a separator; the electrolyte was 1M  $\text{LiPF}_6$  in

---

Ethylene Carbonate (EC), Propylene Carbonate (PC) and Dimethyl Carbonate (DMC) in a 1:1:3 ratio. The pouch cells were sealed under vacuum in a polyethylene coated aluminium film. The cells were cycled using a Biologic VSP galvanostat while being analysed in the X-ray beam. *In situ* XRD patterns were acquired every 3 min while the cell was charging and discharging during 1.5 cycles. This was performed in transmission mode on beamline BM20 at 25 keV ( $\lambda = 0.4956 \text{ \AA}$ ) using an image plate detector. X-ray patterns were refined using FullProf package<sup>15</sup>.

### ***In situ* X-ray Absorption Spectroscopy (XAS)**

*In situ* XAS experiments were performed at the bending magnet based BM30B CRG-10 FAME beamline of the European Synchrotron Radiation Facility (ESRF, Grenoble, France). The storage ring was operated in 7/8+1 mode at 6 GeV with a 200 mA current. Spectra were collected in transmission mode at the Ni (8 333 eV) and Mn K edges (6 539 eV). The beam size (300x150  $\mu\text{m}^2$ ) and the position on the sample were kept constant during the acquisition. Data analysis was performed with Athena and Artemis 15 softwares from the Horae package<sup>16</sup>.

### **XAS Sample preparation**

Nickel and manganese standards with various oxidation states were prepared by diluting the oxides with boron nitride in appropriate proportions and pressed as 5 mm-diameter pellets. The *in situ* measurements were performed in the same electrochemical pouch 20 cells as XRD but with a lower density of electrode (5mg.cm<sup>-2</sup>).

## **Results and discussions**

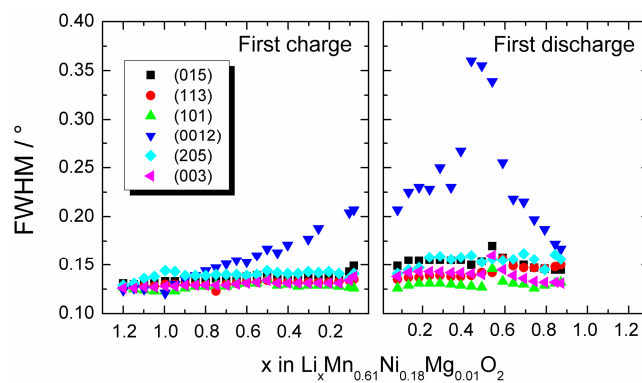
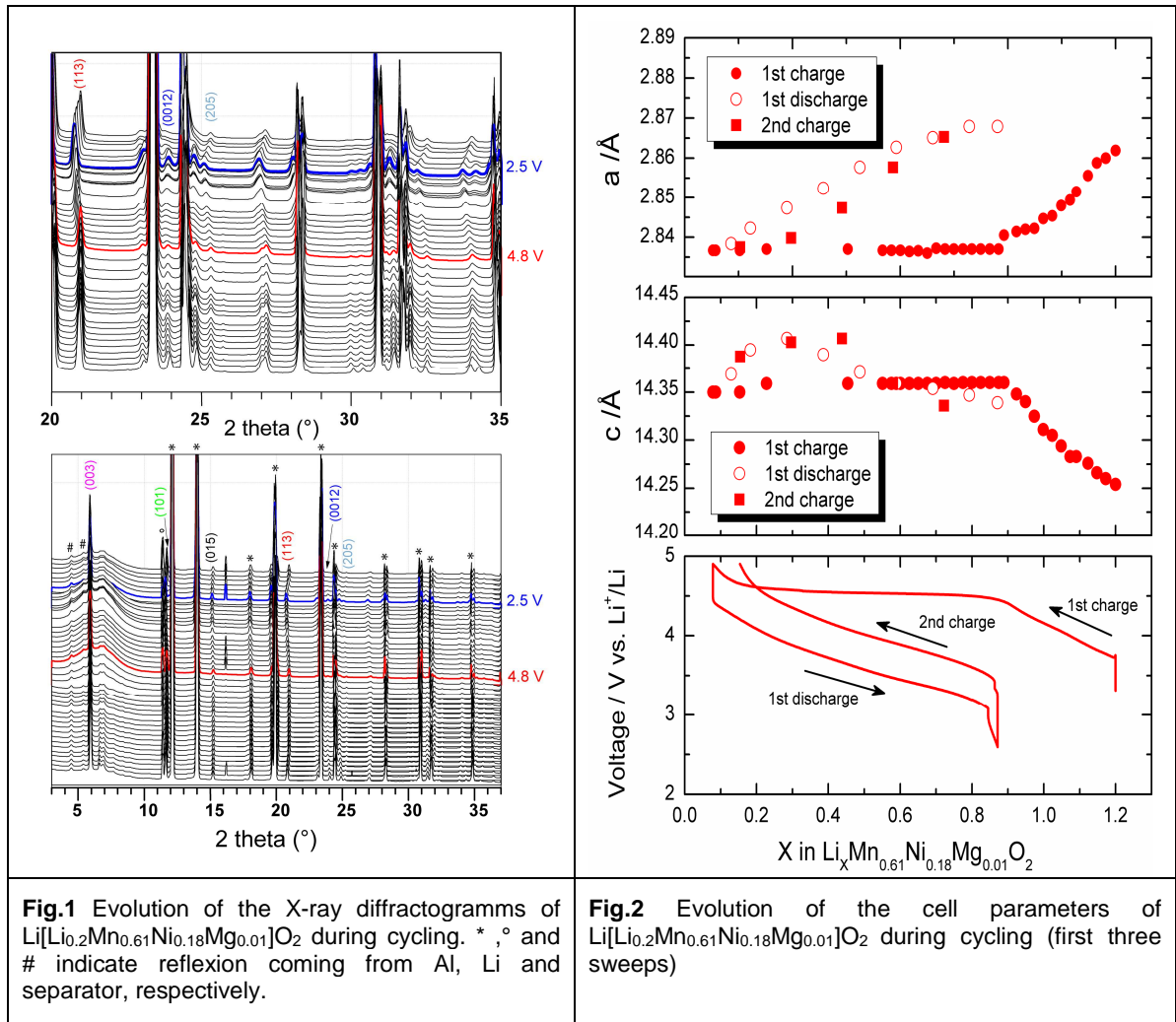
### ***In situ* XRD**

Figure 1 presents the evolution of XRD patterns upon electrochemical cycling. In addition 25 to reflections due to the active materials, several extra phases are observed corresponding to other components of the cell: Aluminium (\*) and Lithium (°). As Al reflections are overlapping with several reflections of the active material, it was not possible to perform a Rietveld refinement. However, the cell parameters evolution was followed using whole pattern matching refinement. For this purpose, the  $R\bar{3}m$  space 30 group was chosen to facilitate comparison with literature. This space group also allows an easy comprehension of the mechanism as *a* and *b* are characterising the slabs and *c* is characterising the interslab distance. The evolution is given on Figure 2.

During the first part of charge corresponding to a monotonous potential increase (1.2 > *x* > 0.9), the cell parameters vary linearly. The decrease of the *a* parameter is 35 usually related to the oxidation of the transition metal in the metallic layer leading to a decrease of their radii. The increase of the *c* parameter is due to the removal of lithium in between the metallic layer that decreases the screening effect between the oxygen layers.

For *x* < 0.9, no further evolution of cell parameters was observed although lithium is still 40 extracted from the material. This behaviour is generally related to a biphasic process. Moreover this corresponds to the plateau in the electrochemical curve that is also commonly attributed to a biphasic process. However no new reflection is observed. A study of the full width at half maximum (FWHM) of the reflections of different (hkl) families was carried out to look for a second phase with cell parameters close from the

ones of the active material.



**Fig.3** Evolution of the FWHM of different hkl families during cycling.

The results are given in Figure 3. The first observation is a large increase of the FWHM of the (0012) reflection during the potential plateau. This could be due to the apparition of stacking faults on the c direction but also to the growth of a reflection due to a second phase close to this reflection. An examination of the FWHM evolution during discharge

shows that the FWHM of the (0012) reflection returns to a value close to the starting one after discharge. As self-healing of stacking fault is very unlikely we believe that the increase of FWHM during charge is due to the apparition of a second phase during this potential plateau Ito et al.<sup>13</sup> already proposed the formation of a spinel phase during this 5 step. Considering this hypothesis, our observation would then fit with the growth of the  $(444)_s$  reflection of a spinel structure with an  $a$  parameter close to 8.25Å. This value is consistent with the one expected for an oxygen deficient spinel, and thus with a loss of oxygen on the plateau. Second charge shows good reversibility during the subsequent cycles. This means that a new structure is created during the first charge and that is 10 reversibly cycled during the following cycles.

### In situ XAS

In order to get a better insight on this possible phase transition, the material was also studied by X-ray absorption spectroscopy. The goal was to reveal local order change accompanying this mechanism which would not be easily seen with X-ray diffraction. 15 XANES analyses were also used in order to follow the evolution of oxidation state of transition metals.

### Nickel XANES

Normalized XANES spectra along charge and discharge at nickel  $K$ -edge are represented on Figure 4. The edge positions are taken at the maximum intensity of each 20 spectrum.

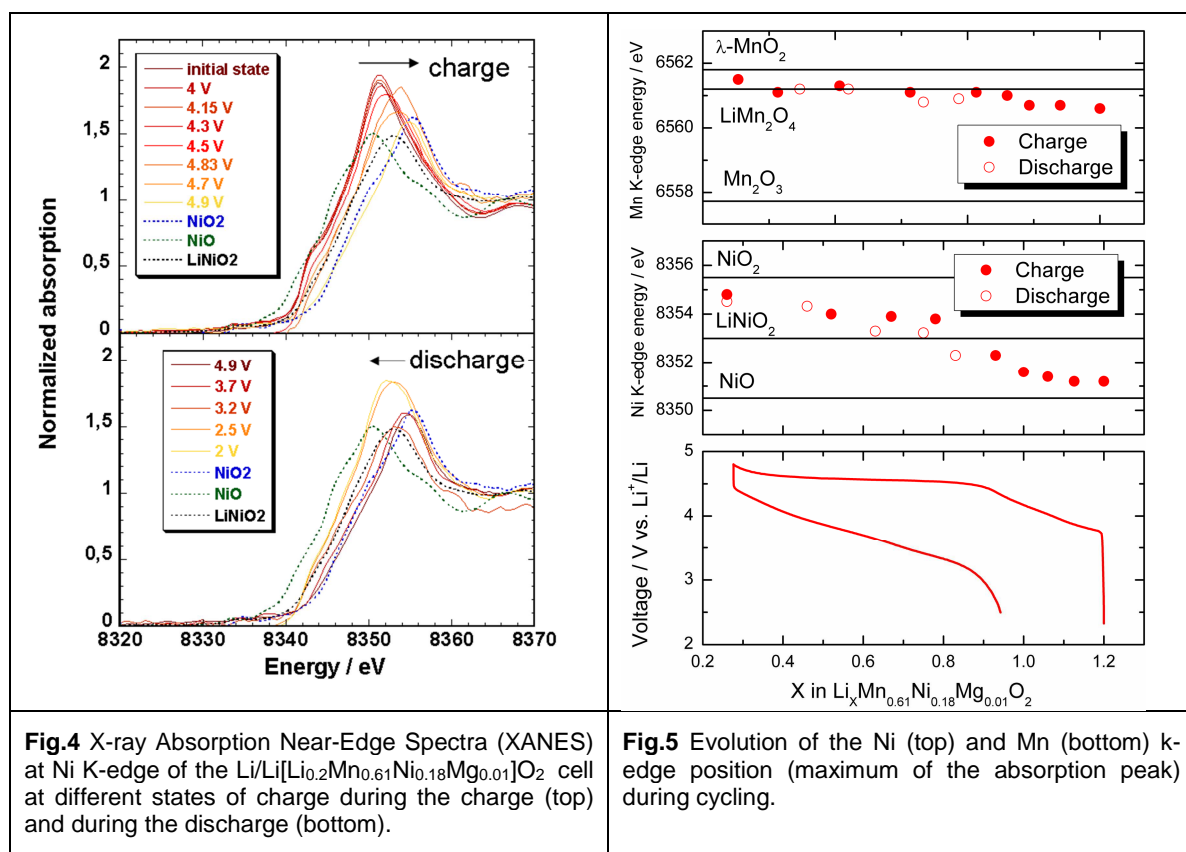


**Fig.4** X-ray Absorption Near-Edge Spectra (XANES) at Ni K-edge of the  $\text{Li}/\text{Li}[\text{Li}_{0.2}\text{Mn}_{0.61}\text{Ni}_{0.18}\text{Mg}_{0.01}]\text{O}_2$  cell at different states of charge during the charge (top) and during the discharge (bottom).

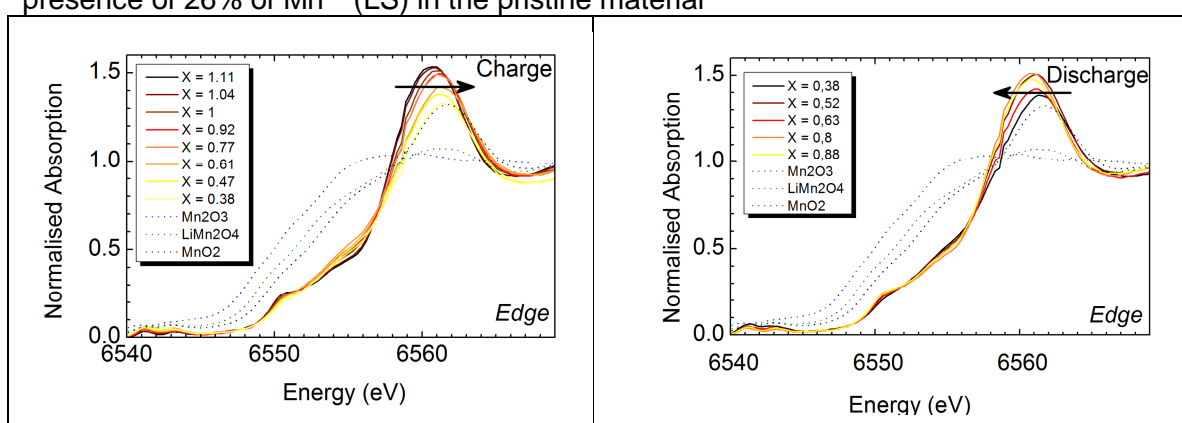
**Fig.5** Evolution of the Ni (top) and Mn (bottom) k-edge position (maximum of the absorption peak) during cycling.

Looking at Figure 5, which provides the evolution of the edge energy as a function of the

Li content, it appears that this energy stays constant around 8351 eV during the first slope of the charge and is starting to increase from about  $x=1$  to  $x=0.8$ . Then this energy seems to stabilise around values in the range of 8354-8354.5 eV up to the fully charged state. The fact that the Ni oxidation state seems to stay 2+ at the beginning of the charge is particularly surprising. The oxidation of  $\text{Ni}^{2+}$  to  $\text{Ni}^{4+}$  is indeed supposed to be the only reaction occurring during this first slope as Mn is believed to be in the 4+ state. Also, the X-ray data are revealing an oxidation of transition metal from the very beginning of the spectra. An explanation would be that our compound is not perfectly stoichiometric and presents a certain fraction of Mn in 3+ oxidation state that would oxidize at the beginning of the charge. A change on the XANES edge of Mn should thus be visible.

### Manganese XANES

Normalized XANES spectra at manganese K-edge during charge and discharge are represented on Figure 6. The estimation of the oxidation state of Mn is not straight forward from the XANES spectra, because several other processes such as structural distortion contribute to the change of shape of the near-edge region of the spectra. These results tend to confirm that an oxidation of the  $\text{Mn}^{3+}$  to  $\text{Mn}^{4+}$  occurs at the very beginning of the charge, before nickel starts to oxidize, in agreement with non-oxidation of Ni at the very beginning of the charge as observed in Ni XANES measurement. The average Mn valence of the starting material is evaluated from the edge crest energy to be close to 3.75+ and reaches 4+ upon charging (Figure 5). However, given the limited accuracy of this determination, a magnetic susceptibility measurement was carried out to determine more accurately the oxidation state of Mn in the starting material. It confirms the presence of 26% of  $\text{Mn}^{3+}$  (LS) in the pristine material



25 **Fig.6** X-ray Absorption Near-Edge Spectra (XANES) at Mn K-edge of the cell at different states of charge during the first charge (left) and subsequent discharge (right).

### Manganese EXAFS

The quality of X-ray absorption spectra at the manganese edge allowed a full analysis of the EXAFS results. The evolution of Mn-O bond length as a function of the state of charge is shown Table 1.

30 It is clearly observed that the first distance which is attributed to Mn-O bonds is shrinking during first part of the charge. This is relevant with the decrease of the  $a$  cell parameter observed by XRD. The oxidation of the transition metal in the metallic layer leads to a decrease of their radii ( $r_{\text{Mn}^{3+}}=0.65\text{\AA}$  and  $r_{\text{Mn}^{4+}}=0.53\text{\AA}$ ). This confirms again that Mn is oxidising at the beginning of the charge.

x	Mn-O (Å)	CN	$\sigma^2$ (Å <sup>2</sup> )	R-factor	x	Mn-O (Å)	CN	$\sigma^2$ (Å <sup>2</sup> )	R-factor
1.2	1.910 ± 0.021	6	0.001746	0,005238	0.61	1.872 ± 0.020	6	0.001600	0,05580
0.92	1.870 ± 0.018	6	0.001040	0,06220	0.47	1.866 ± 0.022	6	0.001837	0,08030
0.77	1.876 ± 0.021	6	0.001580	0,07240	0.38	1.870 ± 0.021	6	0.003008	0,07000

**Table.1** EXAFS results for Mn at different states of charge for Li<sub>1.2</sub>Mn<sub>0.61</sub>Ni<sub>0.18</sub>Mg<sub>0.01</sub>O<sub>2</sub> were CN is coordination number of the first shell and  $\sigma^2$  is the Debye–Waller factor.

## Conclusions

5 Characterisation of the pristine material by XAS and SQUID measurements show that our synthesis leads to a non stoichiometric compound containing Mn<sup>3+</sup> in Low Spin configuration, although this configuration is often considered as unstable. *In situ* XAS demonstrates this Mn<sup>3+</sup> to be electrochemically active during the first charge. The results obtained from *in situ* XRD and XAS tend to show that a new phase is created during the 10 plateau at 4.5 V of the first charge. This new phase should have a close link to the starting phase and could be an oxygen deficient spinel with  $a \approx 8.25\text{Å}$ . The presence of Mn<sup>3+</sup> is often considered as unlikely and the oxidation state of Mn believed to be 4+ *a priori*. This could lead to the mis-interpretation of the data related to this material.

## Acknowledgement

15 We are grateful to the ESRF and CRG committees for providing beam time on lines BM20 and BM30b.

## References

- 1 M. Whittingham, *Chemical Reviews*, 2004, 104, 4271.
- 2 M. Armand and J.-M. Tarascon, *Nature*, 2008, 451, 652.
- 20 3 L. Ji, Z. Lin, M. Alcoutlabi and X. Zhang, *Energy Environ. Sci.*, 2011, 4, 2682.
- 4 M. M. Thackeray, C. S. Johnson, J. T. Vaughey, N. Li, and S. A. Hackney, *Journal of Materials Chemistry*, 2005, 15, 2257.
- 5 C. S. Johnson, J. S. Kim, C. Lefief, N. Li, J. T. Vaughey, and M. M. Thackeray, *Electrochemistry Communications*, 2004, 6, 1085.
- 25 6 A. Ito, D. Li, Y. Ohsawa, and Y. Sato, *Journal of Power Sources*, 2008, 183, 344.
- 7 A. R. Armstrong, M. Holzapfel, P. Novak, C. S. Johnson, S. H. Kang, M. M. Thackeray, and P. G. Bruce, *Journal of the American Chemical Society*, 2006, 128, 8694.
- 8 N. Tran, L. Croguennec, M. Menetrier, F. Weill, P. Biensan, C. Jordy, and C. Delmas, *Chemistry of Materials*, 2008, 20, 4815.
- 30 9 F. La Mantia, F. Rosciano, N. Tran and P. Novak, *Journal of the Electrochemical Society*, 2009, 156, A823.
- 10 J. Hong, D.-H. Seo, S.-W. Kim, H. Gwon, S.-T. Oh, and K. Kang, *J. Mater. Chem.*, 2010, 20, 10179.
- 11 N. Yabuuchi, K. Yoshii, S.-T. Myung, I. Nakai, and S. Komaba, *Journal of the American Chemical Society*, 2011, 133, 4404.
- 35 12 A. Ito, D. Li, Y. Sato, M. Arao, M. Watanabe, M. Hatano, H. Horie, and Y. Ohsawa, *Journal of Power Sources*, 2010, 195, 567.
- 13 A. Ito, K. Shoda, Y. Sato, M. Hatano, H. Horie, and Y. Ohsawa, *Journal of Power Sources*, 2011, 196, 4785.
- 40 14 A. Ito, Y. Sato, T. Sanada, M. Hatano, H. Horie, and Y. Ohsawa, *Journal of Power Sources*, 2011, 196, 6828.
- 15 J. Rodríguez-Carvajal, *Physica B: Condensed Matter*, 1993, 192, 55.
- 16 B. Ravel and M. Newville, *Journal of Synchrotron Radiation*, 2005, 12, 537.
- 17 R. Prasad, R. Benedek, A. J. Kropf, C. S. Johnson, A. D. Robertson, P. G. Bruce, and M. M. Thackeray, *Phys. Rev. B*, 2003, 68, 012101.
- 45 18 Z.-F. Huang, F. Du, C.-Z. Wang, D.-P. Wang, and G. Chen, *Phys. Rev. B*, 2007, 75, 054411.
- 19 A. Manceau, A. I. Gorskov, and V. I. Drits, *American Mineralogist*, 1992, 77, 1133.